Journal of Medicinal Chemistry

pubs.acs.org/jmc

Article

GPCR Agonist-to-Antagonist Conversion: Enabling the Design of Nucleoside Functional Switches for the A_{2A} Adenosine Receptor

Anna Shiriaeva,[○] Daejin Park,[○] Gyudong Kim,[○] Yoonji Lee,[○] Xiyan Hou, Dnyandev B. Jarhad, Gibae Kim, Jinha Yu, Young Eum Hyun, Woomi Kim, Zhan-Guo Gao, Kenneth A. Jacobson, Gye Won Han, Raymond C. Stevens, Lak Shin Jeong,* Sun Choi,* and Vadim Cherezov*

Cite This: *J. Med. Chem.* 2022, 65, 11648–11657

Read Online

ACCESS | Metrics & More | Article Recommendations | Supporting Information

ABSTRACT: Modulators of the G protein-coupled A_{2A} adenosine receptor (A_{2A}AR) have been considered promising agents to treat Parkinson's disease, inflammation, cancer, and central nervous system disorders. Herein, we demonstrate that a thiophene modification at the C8 position in the common adenine scaffold converted an A_{2A}AR agonist into an antagonist. We synthesized and characterized a novel A_{2A}AR antagonist, **2** (LJ-4517), with K_i = 18.3 nM. X-ray crystallographic structures of **2** in complex with two thermostabilized A_{2A}AR constructs were solved at 2.05 and 2.80 Å resolutions. In contrast to A_{2A}AR agonists, which simultaneously interact with both Ser277$^{7.42}$ and His278$^{7.43}$, **2** only transiently contacts His278$^{7.43}$, which can be direct or water-mediated. The *n*-hexynyl group of **2** extends into an A_{2A}AR exosite. Structural analysis revealed that the introduced thiophene modification restricted receptor conformational rearrangements required for subsequent activation. This approach can expand the repertoire of adenosine receptor antagonists that can be designed based on available agonist scaffolds.

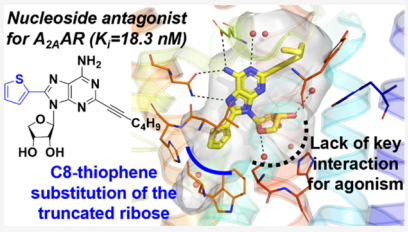

INTRODUCTION

Adenosine is an endogenous nucleoside necessary for the proper response to the stress of every organ in our body. It is an essential component as a precursor of intracellular nucleic acids such as RNA and also functions extracellularly as a neuromodulator through four adenosine receptor (AR) subtypes, i.e., A_1, A_{2A}, A_{2B}, and A_3.[1] As prototypical G protein-coupled receptors (GPCRs), the ARs have seven transmembrane helical domains that transduce signals from the outside to the inside of the cell, playing a regulatory role in the central nervous, cardiovascular, and immune systems.[2] To discover AR modulators, modification of the adenosine scaffold has been a key strategy. As nucleoside analogs are generally safe, are well tolerated *in vivo*, and offer versatile and drug-like scaffolds for diverse protein targets, they have been applied as useful templates for drug discovery. Although there are several critical issues that limit their clinical efficiency, including poor selectivity and stability, side effects, and suboptimal therapeutic efficacy, nucleoside analogs have been widely applied as traditional chemotherapeutic or antiviral drugs.[3] Over 40 nucleoside drugs are already on the market as therapeutic agents.[4]

In the case of A_{2A}AR, nucleoside agonists have been developed as anti-inflammatory agents; however, numerous A_{2A}AR agonists for peripheral anti-inflammatory action have failed in clinical trials, partly due to cardiovascular side effects of receptor activation.[2] A_{2A}AR antagonists have been considered as potential candidates for the treatment of neurodegenerative disorders,[5−7] and recently, they have gained importance in the immunotherapy of cancer.[8,9] Historically, A_{2A}AR antagonists have been primarily designed based on a xanthine scaffold that mimics the binding mode of the adenine core in the ligand-binding pocket.[10] The presence of a sugar moiety has been traditionally considered a specific feature of an A_{2A}AR agonist, and the nucleoside scaffold has never been used for the design of A_{2A}AR antagonists. Although various A_3AR nucleoside agonists can readily be modified to reduce efficacy and act as antagonists by truncating the ribose moiety[11] or by applying subtle chemical modification to the ribosyl group,[12] these approaches have not been successful for A_{2A}AR nucleoside ligands until now.

Interestingly, the first X-ray crystallographic structure of A_{2A}AR in complex with an antagonist, ZM-241385, showed that in the inactive-state receptor, the sugar-binding subpocket is open with a volume quite amenable for ligand modification and can be potentially targeted by a structure-based design approach.[13] Furthermore, when the first A_{2A}AR agonist-bound structure was solved, it demonstrated that the receptor could be trapped in both inactive and active-like states in the absence of intracellular signaling partners. It was revealed that A_{2A}AR activation involves shifts of helices V, VI, and VII on the

Received: March 24, 2022
Published: August 17, 2022

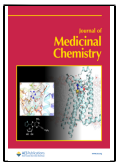

https://doi.org/10.1021/acs.jmedchem.2c00462
J. Med. Chem. 2022, 65, 11648−11657

intracellular side.[14] We hypothesized that an appropriately designed ribose moiety combined with a specific feature of an antagonist could provide a nucleoside-derived A_{2A}AR antagonist. Considering that nucleosides represent a well-validated class of potential drug candidates, a systematic approach to designing A_{2A}AR antagonists based on a nucleoside scaffold could provide a viable template for new anticancer or cerebroprotective agents.

Here, we report a newly discovered A_{2A}AR antagonist with a 4′-hydroxymethyl-truncated nucleoside scaffold. The C8-substitution of the adenine moiety of a nucleoside agonist (**1**) converted the ligand into an antagonist (**2**). Thus, we determined two X-ray crystal structures of A_{2A}AR in complex with compound **2** and performed molecular dynamics (MD) simulation to investigate how this new type of antagonist interacts with the receptor. We also revealed how the compound acts as an antagonist despite containing a sugar moiety, a known characteristic of A_{2A}AR agonists. These results may provide an additional rationale for various pharmacologically selective ligand designs for this and other GPCRs.

RESULTS AND DISCUSSION

Design and Synthesis of a New Nucleoside A_{2A}AR Antagonist, 2 (LJ-4517). Our previous structure−activity relationship (SAR) study identified compound **1** as a potent A_{2A}AR agonist with a rigid C2-substituent (Figure 1, left).[15]

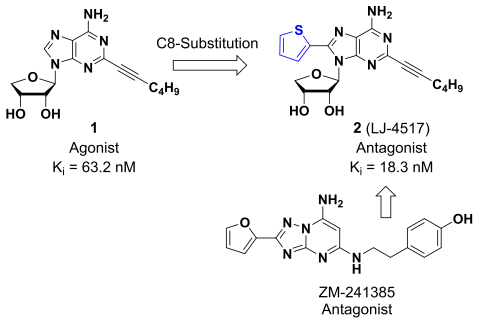

Figure 1. Design of the A_{2A}AR antagonist **2** from an agonist scaffold and the antagonist ZM-241385. The introduced thiophene group (blue), which is isosteric to the furan group of ZM-241385, changed the ligand's mode of action from agonism to antagonism.

Despite the lack of a 4′-hydroxymethyl group, this compound showed the ability to fully activate A_{2A}AR. According to a large number of X-ray structures, the adenosine receptor binding requires a $\pi-\pi$ stacking between the flat heterocycles, such as the adenine ring, and the conserved Phe residue (Phe168$^{5.29}$ in A_{2A}AR; superscripts refer to Ballesteros−Weinstein residue numbering[16]) in the binding site.

Since many A_{2A}AR antagonists, such as ZM-241385, have an aryl ring substitution at the C8 position of the adenine or adenine-like moiety, we speculated that a C8-substitution of **1** mimicking the furan group of ZM-241385 might produce an antagonistic effect or, at least, increase the binding affinity. Based on these two strategies, we designed and synthesized a new ligand **2** (Figure 1, right), modifying the adenine scaffold with an 8-thien-2-yl group. Truncated 4′-oxoadenosine derivative **2** was synthesized from D-erythrono-1,4-lactone, as shown in Scheme 1. Successfully, the introduction of the thiophene group converted an agonist, i.e., compound **1**, into a more potent neutral antagonist **2** (Table 1). It also showed a similar binding affinity for A_3AR (K_i = 15.6 ± 1.6 nM), while it showed 20−40-fold less affinity for A_1AR (K_i = 392 ± 99.4 nM) and A_{2B}AR (K_i = 834 ± 10.6 nM). A furan-substituted analog on the C8 position was also synthesized and tested (K_i = 18.0 ± 5.5 nM for A_{2A}AR) but did not show better affinity than that of **2**.

Scheme 1. Synthesis of the Truncated 2-Hexynyl-8-thien-2-yl-adenosine (Compound 2)[a]

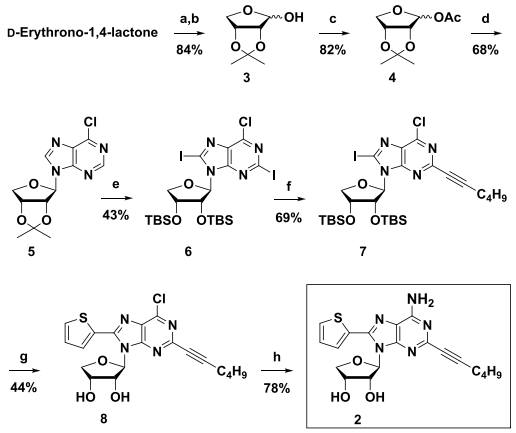

[a]Reagents and conditions: (a) *p*TSA, 2,2-dimethoxypropane, DMF, 4 h, 100 °C; (b) DIBAL-H, toluene, −78 °C, 30 min; (c) Ac_2O, pyridine, rt, 3 h; (d) 6-chloropurine, HMDS, $(NH_4)_2SO_4$, TMSOTf, 1,2-dichloroethane, 0 to 80 °C, 15 h; (e) (i) 1 N HCl, THF, rt, 15 h; (ii) TBSCl, imidazole, DMF, rt, 15 h; (iii) tetramethylpiperidine, I_2, *n*-BuLi, THF, −78 °C, 5 h; (f) $Pd(PPh_3)_4$, Cs_2CO_3, CuI, 1-hexyne, DMF, rt, 5 h; (g) (i) $PdCl_2(PPh_3)_2$, 2-tributylstannylthiophene, THF, 60 °C, 1 h; (ii) Et_3N, $Et_3N{\cdot}3HF$, THF, rt, 15 h; (h) NH_3/*t*-BuOH, 100 °C, 12 h.

Crystal Structure of A_{2A}AR in Complex with Compound 2. To elucidate the binding mode of this new nucleoside antagonist and explain the change in its mode of action, we attempted to solve the crystal structure of A_{2A}AR in complex with **2**. After initial failure using the A_{2A}AR-*b*RIL construct,[17] we succeeded in obtaining cocrystals (Figure S1) in complex with **2** using the thermostabilized A_{2A}AR-STaR2-*b*RIL[18] and solved its structure at 2.05 Å resolution (Figure 2 and Table S1).

Compound **2** contains three functional moieties appended on its adenine nucleobase: (i) a 4′-hydroxymethyl-truncated ribosyl (oxolane-3,4-diol) moiety at N9, (ii) an *n*-hexynyl group at position C2, and (iii) a thiophene group at C8. The adenine scaffold of **2** is coordinated in the binding pocket by two hydrogen bonds with Glu169$^{5.30}$ and Asn253$^{6.55}$ and by a $\pi-\pi$ stacking interaction with Phe168$^{5.29}$ (Figure 2C,D). These interactions are common for other A_{2A}AR ligands and have been observed in both agonist- and antagonist-bound structures.[14,19]

The ribose-like moiety of **2** in our structure adopts a South conformation and is rotated at approximately 70° when compared with the North conformation of the ribose group of the agonist NECA (Figure 3). The 3′-OH group forms a hydrogen bond with His278$^{7.43}$ (bond length of 2.9 Å), while in agonist-bound A_{2A}AR structures, both 2′-OH and 3′-OH form hydrogen bonds with His278$^{7.43}$ and Ser277$^{7.42}$, respectively (Figure 3A).[14,19] The thermostabilized A_{2A}AR-STaR2-*b*RIL receptor, however, lacks the critical residue Ser277$^{7.42}$, which is mutated to alanine in this construct.

https://doi.org/10.1021/acs.jmedchem.2c00462
J. Med. Chem. 2022, 65, 11648−11657

Table 1. Binding Affinity and Potency of Compound 2 at WT and Mutants of $A_{2A}AR$[a]

	WT	S227A	H278A	S277A/H278A
K_d of [^{3}H]ZM-241385 (nM)	1.95 ± 0.15	1.8 ± 0.2	2.9 ± 1.1	2.7 ± 0.9
B_{max} of [^{3}H]ZM-241385 (pmol mg^{-1} protein)	2.03 ± 0.17	2.2 ± 0.3	2.4 ± 0.3	2.1 ± 0.5
K_i of compound **2** (nM)	18.3 ± 4.8	21.6 ± 7.7	19.0 ± 3.3	56.4 ± 9.6
EC_{50} of agonist (nM)[b]	0.9 ± 0.3	94 ± 38	109 ± 24	8390 ± 490
fold shift of agonist concentration−response curves of 300 nM **2**[b]	28.6 ± 3.4	25.0 ± 3.9	26.2 ± 4.7	4.8 ± 1.8

[a]Results are expressed as mean ± standard error of the mean (SEM) from three to four independent experiments. [b]cAMP accumulation using CGS21680 as an agonist.

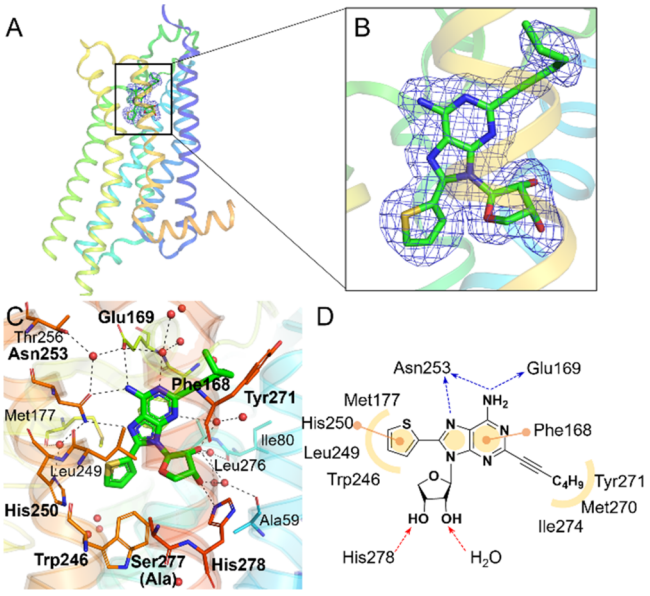

Figure 2. Structure of $A_{2A}AR$-StaR2-*b*RIL in complex with compound **2** (PDB ID: 8CU7). (A) Overall receptor structure with helices shown as a rainbow-colored cartoon and **2** shown as green sticks. (B) Conformation of **2** within the ligand-binding pocket. The mFo-DFc ligand-omit electron density map contoured at 3σ is shown as a blue mesh. (C) Details of the receptor−ligand interactions. Hydrogen bond interactions of **2** with $A_{2A}AR$ residues are highlighted in black dashed lines. Water molecules are shown as red spheres. (D) Schematic diagram of ligand-interacting residues. Hydrogen bonds are shown as blue and red dashed arrows, and $\pi-\pi$ stacking interactions are displayed as orange lines with filled circles at both ends. Hydrophobic interactions are colored in light orange.

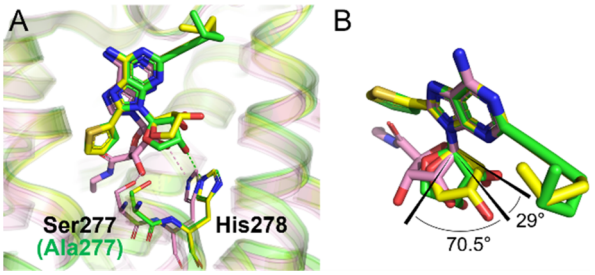

Figure 3. Conformation of the ribose-like moiety in the antagonist **2** and the agonist NECA bound to $A_{2A}AR$. (A) Superimposed crystal structures of **2** bound to $A_{2A}AR$-STaR2-*b*RIL (green; PDB ID: 8CU7) and $A_{2A}AR$-STaR2-S277-*b*RIL (yellow; PDB ID: 8CU6) and NECA bound to the thermostabilized $A_{2A}AR$ (pink; PDB ID: 2YDV[19]). The antagonist **2** (green) can form only one hydrogen bond (green dashed line) with His278$^{7.43}$ of $A_{2A}AR$, while the agonist NECA (pink) forms two hydrogen bonds (pink dashed lines) with both Ser277$^{7.42}$ and His278$^{7.43}$. (B) Differences in dihedral angles between conformations of the ribose-like motif of **2** in $A_{2A}AR$-STaR2-*b*RIL (green) and $A_{2A}AR$-STaR2-S277-*b*RIL (yellow) when compared with the agonist NECA (pink; PDB ID: 2YDV[19]). The ligands are superimposed by their common adenine scaffold.

Therefore, we restored this residue back to S277$^{7.42}$ (construct $A_{2A}AR$-STaR2-S277-*b*RIL), crystallized the new construct in complex with **2** (Figure S1), and solved its structure at 2.80 Å resolution (Table S1).

In the structure with the restored S277$^{7.42}$ residue, the truncated sugar moiety of **2** switched to a North conformation and rotated further away by additional 29° (Figure 3B), making it hard to reach and interact with Ser277$^{7.42}$ or His278$^{7.43}$ (Figure 3A). Thus, in both complex structures, the truncated sugar moiety is sterically displaced from the agonist-like position by the thiophene group, which prevents simultaneous engagement with Ser277$^{7.42}$ and His278$^{7.43}$ that are critical for receptor activation.[20,21]

Structural analysis showed that agonist-bound and antagonist-bound $A_{2A}AR$ structures have significantly different binding cavity surfaces (Figure 4 and Figure S2). In the agonist-bound structures, the ribose-like moiety maintains the hydrogen bonding with the critical residues in the bottom pocket and pulls helices V, VI, and VII inward, shrinking the deep orthosteric binding site cavity (Figure 4A, see the blue dashed arrows). Only one or two water molecules were observed in this deep pocket in the available structures (Figure S2A). In contrast, antagonist-bound $A_{2A}AR$ structures consistently showed a much larger binding cavity at the bottom of the ligand-binding pocket (Figure 4B,C). The antagonist molecules rarely form hydrogen bonding with the deeper residues so that they cannot induce the movements of TM helices. The empty bottom pockets in the antagonist-bound structures tend to be filled with water molecules. Some antagonists, such as AZD4635 (PDB ID: 6GT3[22]) or compound **4e** (PDB ID: 5OLZ[23]), can occupy this bottom pocket but do not make direct hydrogen bonding interaction with its hydrophilic residues (Figure S2B).

In addition, the *n*-hexynyl group of **2** extends into an exosite that was recently described in the structure of $A_{2A}AR$ with an antagonist LUAA47070 (PDB ID: 5OLV).[23] This exosite can also accommodate aromatic groups, for example, 2-methylaniline group of Vipadenant (PDB ID: 5OLH)[23] or 2-methoxyphenyl group of Cmpd-1 (PDB ID: 5UIG).[25] In contrast, in the structure of $A_{2A}AR$ in complex with ZM-241385 (PDB IDs: 4EIY, 6WQA, etc.),[17,24] the hydroxyphenol group of the ligand points away from the exosite, facing toward the solvent-exposed surface, while the sidechain of Tyr271$^{7.36}$ switches its conformation, closing the exosite and engaging in an interaction with ZM-241385 through a bridging water molecule (Figure 4).

Functional Characterization of Compound 2. To investigate the role of the key residues (i.e., Ser277$^{7.42}$ and

https://doi.org/10.1021/acs.jmedchem.2c00462
J. Med. Chem. 2022, 65, 11648−11657

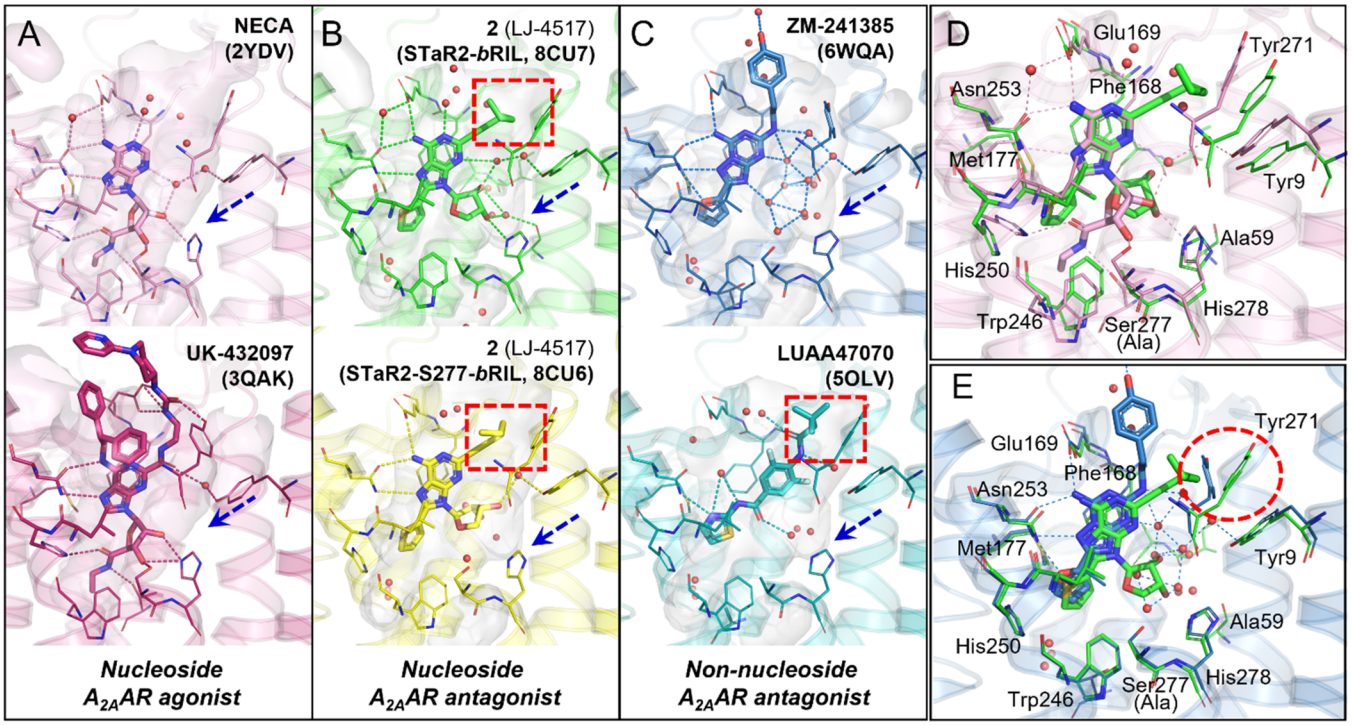

Figure 4. Comparison of the binding sites of A_{2A}AR in complex with nucleoside agonists, nucleoside antagonists, and non-nucleoside antagonists. (A) Surface representation of the A_{2A}AR binding pocket with nucleoside A_{2A}AR agonists, NECA (pink; PDB ID: 2YDV[19]) and UK-432097 (plum; PDB ID: 3QAK[14]). (B) Surface representation of A_{2A}AR with **2** in the A_{2A}AR-STaR2-*b*RIL construct (green; PDB ID: 8CU7) and A_{2A}AR-STaR2-S277-*b*RIL construct (yellow; PDB ID: 8CU6). The *n*-hexynyl group of **2** extends into the exosite enclosed in a red dashed box. (C) Surface representation of A_{2A}AR with non-nucleoside antagonists, ZM-241385 (sky blue; PDB ID: 6WQA[24]) and LUAA47070 (teal; PDB ID: 5OLV[23]). In the ZM-241385-bound structure, the exosite is closed due to a switched conformation of Tyr271$^{7.36}$. LUAA47070 and **2** extend in the "open" exosite. Water molecules in binding pockets are shown as red spheres. (D) Superposition of **2** (green; A_{2A}AR-STaR2-*b*RIL construct; PDB ID: 8CU7) and the agonist NECA (pink; PDB ID: 2YDV[19]) in the ligand-binding pocket of A_{2A}AR. (E) Superposition of **2** (green; A_{2A}AR-STaR2-*b*RIL construct; PDB ID: 8CU7) and ZM-241385 (sky blue; PDB ID: 6WQA[24]) in the binding pocket of A_{2A}AR illustrating the conformational difference of Tyr271$^{7.36}$ (marked in a red dashed circle).

His278$^{7.43}$) in the interaction with **2** and its mode of action, we performed competition radioligand binding and cAMP accumulation assays using the wild-type (WT) A_{2A}AR, its mutants S277$^{7.42}$A and H278$^{7.43}$A, and the double mutant S277$^{7.42}$A/H278$^{7.43}$A (Figure 5 and Table 1). We constructed CHO cell lines stably expressing the S277$^{7.42}$A, H278$^{7.43}$A, and S277$^{7.42}$A/H278$^{7.43}$A mutant receptors at similar expression levels to those of WT A_{2A}AR. Receptor expression levels were quantified based on the B_{max} values from saturation binding experiments using the A_{2A}AR antagonist radioligand [^{3}H]ZM-241385 (Table 1).

First, we confirmed that the applied mutations did not affect the binding of the radioligand antagonist [^{3}H]ZM-241385 (Table 1). Compound **2** was shown to be potent in displacing the binding of [^{3}H]ZM-241385 at WT A_{2A}AR. Neither S277$^{7.42}$A nor H278$^{7.43}$A alone could impact the binding affinity of **2**, whereas the double mutant S277$^{7.42}$A/H278$^{7.43}$A decreased the binding affinity of **2** by approximately 3-fold (Table 1 and Figure 5A). Second, we confirmed that the selective A_{2A}AR agonist CGS21680[19] functions as an agonist for the A_{2A}AR mutants in the G_s protein-mediated cAMP accumulation assay (Figure 5C). As expected for an agonist, the potency of CGS21680 was reduced by approximately two orders of magnitude on binding to S277$^{7.42}$A or H278$^{7.43}$A mutants and further decreased by ~100-fold on the double mutant S277$^{7.42}$A/H278$^{7.43}$A (Figure 5C and Table 1).

To determine the antagonistic activity of **2**, we assayed the cAMP accumulation induced by CGS21680 in the presence and absence of 300 nM **2** (Figure 6). No activity for **2** in the cAMP assays was observed at WT or mutants of A_{2A}AR (Figure 5B). **2** shifted the CGS2180 concentration−response curves to higher concentrations to a similar extent as observed in WT (28.6-fold), S277$^{7.42}$A (25.0-fold), and H278$^{7.43}$A (26.2-fold) but to a lesser extent (4.8-fold) in the double mutant S277$^{7.42}$A/H278$^{7.43}$A (Figure 6 and Table 1).

Taken together, we established that **2** functions as an antagonist of A_{2A}AR. The double mutation of S277$^{7.42}$ and H278$^{7.43}$ affected the binding of **2** but did not impact the binding of ZM-241385, thereby suggesting that interactions of **2** with S277$^{7.42}$ and H278$^{7.43}$ contribute to the binding affinity of this ligand but do not induce signaling. In addition, the 2.05 Å A_{2A}AR-StaR2-*b*RIL crystal structure contains an allosteric Na^+ ion bound in the sodium binding site (Figure S3). Since many other high-resolution inactive GPCR structures contain Na^+ in the sodium binding site while the sodium site is collapsed in the known active-like GPCR structures,[17] this also proves that the structure is an inactive form bound with **2**.

Insights into the Ligand Binding Mode at A_{2A}AR. Based on the analysis of available A_{2A}AR structures, receptor activation was found to be triggered by simultaneous interactions of an agonist with residues Phe168$^{5.29}$, Glu169$^{5.30}$, Asn253$^{6.55}$, Ser277$^{7.42}$, and His278$^{7.43}$.[26] Although **2** has a ribose-like group, known as a typical agonist feature,

https://doi.org/10.1021/acs.jmedchem.2c00462
J. Med. Chem. 2022, 65, 11648−11657

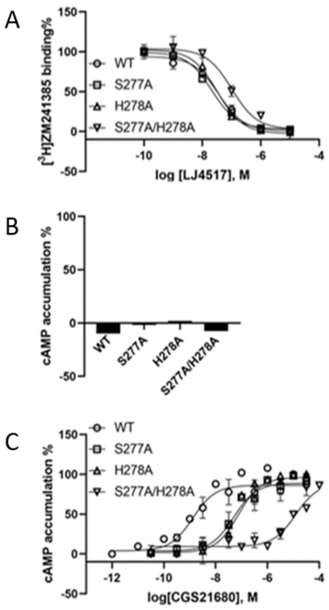

Figure 5. Effects of S277$^{7.42}$A and H278$^{7.43}$A mutations on ligand binding and signaling at A_{2A}AR. (A) Displacement of [^{3}H]ZM-241385 (1.2 nM) by **2** at WT A_{2A}AR and its mutants. The K_i values from three independent experiments are shown in Table 1. (B) cAMP accumulation induced by 10 μM **2**. Results are normalized by the signal induced by 10 μM forskolin and are expressed as mean ± standard deviation (SD) from three independent experiments. (C) cAMP accumulation in CHO cells expressing WT or mutants of A_{2A}AR as a function of increasing concentration of the agonist CGS21680. The signal is normalized by the level of cAMP accumulation induced by 10 μM forskolin. Individual points represent mean ± SD from four independent experiments.

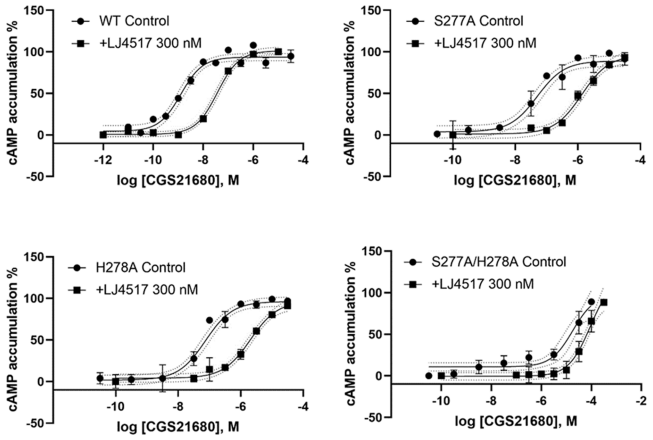

Figure 6. Effects of S277$^{7.42}$A and H278$^{7.43}$A mutations on A_{2A}AR signaling in the absence and presence of **2**. It shows antagonistic properties at the WT receptor and S277$^{7.42}$A and H278$^{7.43}$A mutants. Mutations of both residues S277$^{7.42}$ and H278$^{7.43}$ can disrupt A_{2A}AR signaling. Results are expressed as mean ± SD from three to four independent experiments. The cAMP accumulation in CHO cells expressing WT or mutant receptors induced by 10 μM forskolin was expressed as 100%.

the conformation of this group in the receptor's binding pocket was altered by steric hindrance from the thiophene group, preventing it from engaging in interactions with both Ser277$^{7.42}$ and His278$^{7.43}$. This could explain why **2** acts as an antagonist, whereas its analog, compound **1**, lacking the thiophene group at the C8 position,[15] functions as an agonist.

Another common feature among the majority of A_{2A}AR agonists and antagonists with substitutions at the C2 position is the rigidity of the extended scaffolds. Compound **2**'s analogs with more flexible groups at the C2 position, for example, 2-hexenyl or hexanyl, display 10−100-fold lower A_{2A}AR affinities compared to analogs with a 2-hexynyl group.[15] It is possible that the rigidity of the C8-substituted adenine scaffold contributes to both affinity and antagonism of A_{2A}AR by restricting activation-related movements of TM helices.

MD Simulation of Compound 2's Interactions with A_{2A}AR. Long-timescale (1000 ns) MD simulation of **2** in the binding pocket of A_{2A}AR provides additional insights into the binding mode of **2** (Figure 7). As shown in Video S1 (Supporting Information), the introduced thiophene group stably occupied a hydrophobic subpocket in the bottom part of the ligand-binding site. Furthermore, the truncated ribose moiety of **2** could rotate around its bond with the adenine scaffold (Figure 7A) and establish transient contacts with His278$^{7.43}$ (Figure 7B−D). Interestingly, direct hydrogen bonding between the ligand and His278$^{7.43}$ was formed in only ∼5% of the simulated time points, while water-mediated hydrogen bonding was additionally observed in ∼41% of snapshots (Figure 7C).

Therefore, we suggest two potential explanations as to why the contact of **2** with His278$^{7.43}$ alone does not induce signaling. First, the contact is kinetically unstable to cause the activation-related helical rearrangement, and second, such a rearrangement can be sterically restricted by the thiophene group of **2**. While the truncated ribose moiety of **2** appears to nicely occupy the bottom pocket, the C8-thiophene group makes a steric hindrance to avoid tight interactions with the critical residues for agonism so that the compound acts as a neutral antagonist for A_{2A}AR despite its agonist-like scaffold. We further speculate that the 4′-hydroxymethyl truncation of the ribose ring reduces the steric crowding in the binding site, making it possible to apply a C8-aryl substitution to produce a potent nucleoside antagonist.

CONCLUSIONS

We synthesized and characterized a new nucleoside A_{2A}AR antagonist **2**, which was designed by introducing a thiophene group at the C8 position of an agonist scaffold. To rationalize the change in the ligand's mode of action, we determined the crystal structures of **2** in complex with two thermostabilized A_{2A}AR constructs and conducted MD simulations. In contrast to A_{2A}AR agonists, which interact with both Ser277$^{7.42}$ and His278$^{7.43}$ simultaneously, **2** formed transient contacts only with His278$^{7.43}$, which can be direct or water-mediated.

To activate the receptor, the ligand must attain a suitable conformation to engage with conserved polar, hydrogen bonding residues deep in the orthosteric binding pocket.[26,27] This interaction results in the conformational reorganization of the transmembrane helices V, VI, and VII required for receptor activation. We hypothesized that aromatic or bulky rigid groups at position C8 could restrict activation-related movements of receptor helices so that the ligand does not contact Ser277$^{7.42}$ or His278$^{7.43}$, or such contacts do not lead to signaling. Aryl substitutions at the C8 position have been successfully applied for many nucleobase analogs previously but not for ribose-containing A_{2A}AR agonists. By introducing a thiophene group at the C8 position, we have achieved this previously unattainable goal of disrupting A_{2A}AR activation while maintaining a contribution of the ribose-like moiety for

https://doi.org/10.1021/acs.jmedchem.2c00462
J. Med. Chem. 2022, 65, 11648−11657

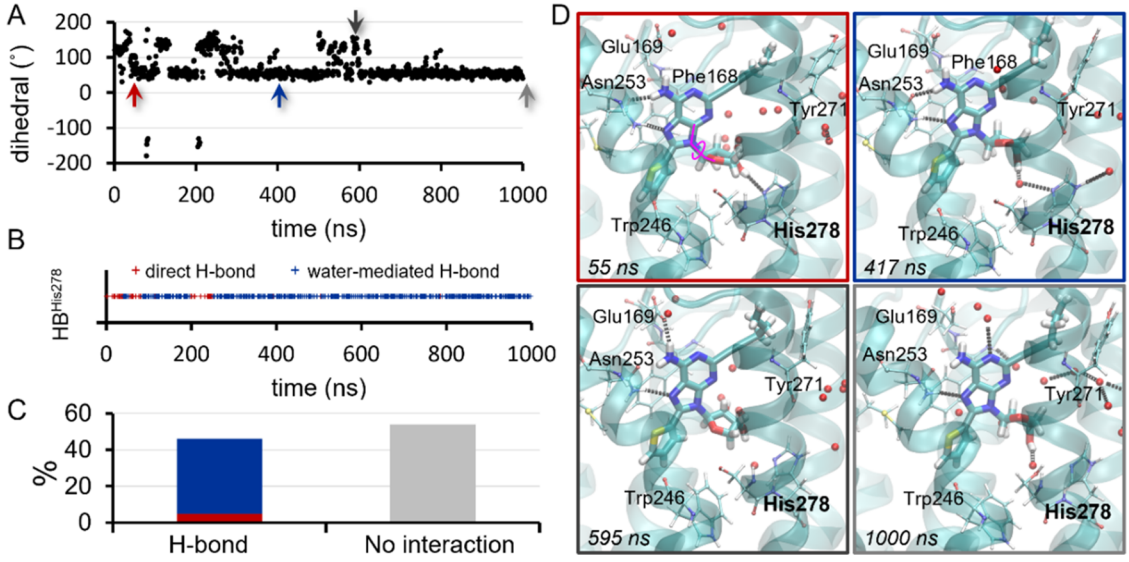

Figure 7. Transient interactions between **2** and His278$^{7.43}$ revealed by MD simulations. (A) Time evolution of the dihedral angle formed by the adenine and ribose rings (marked by magenta lines in D). (B) Hydrogen bond formation between **2** and His278$^{7.43}$. The direct interaction is indicated in red, while the indirect (water-mediated) interaction is indicated in blue. (C) Percentage of snapshots where direct hydrogen bonds (red), water-mediated hydrogen bonds (blue), or no interaction (gray) was observed between the ligand and His278$^{7.43}$. (D) Representative snapshots of the ligand binding interactions during the MD simulation. The receptor structure is displayed as a transparent ribbon. Compound **2** and the interacting residues are represented as thick and thin sticks, respectively. The water molecules near the ligand (within 4 Å) are shown as red spheres. Hydrogen bonds are shown as dashed lines.

increasing binding affinity. For the future work, analogs with several substituents including alkyl or phenyl are under investigation to cover full SAR analysis on C8-aryl-substituted analogs. Our finding that the introduction of a single functional group can shift the ligand's mode of action from agonism to antagonism therefore presents the possibility of designing molecular switches that can modulate receptor activation.

EXPERIMENTAL SECTION

General Procedures. ^{1}H NMR and ^{13}C NMR spectra were measured by a Jeol JNM-ECZ 400s (400 MHz/100 MHz), Bruker AV500 (500 MHz), or Bruker AV800 (800 MHz/200 MHz) spectrometer in $CDCl_3$, CD_3OD, or DMSO-d_6, and chemical shifts are reported as parts per million (δ) relative to the solvent peak. Coupling constants (J) are reported in hertz (Hz). Melting points were obtained by a Barnstead Electrothermal 9100 instrument. Optical rotations were measured in a Jasco-P2000 in CH_3OH or DMSO. The UV spectra were determined on a PerkinElmer Lambda25 in CH_3OH. Elemental analyses (C, H, and N) were used to determine the purity of all synthesized compounds, and the results were within ±0.4% of the calculated values, confirming ≥95% purity. High-performance liquid chromatography (Agilent, 1260 Infinity) was also performed to determine the purity of the final compound **2**, whose purity was >99%. The sample in acetonitrile was injected to HPLC with a ZORBAX Eclipse XDB-C18 (5.0 μm, 4.6 × 250 mm) column. The mobile phase was a mixture of acetonitrile (A) and 0.01 M KH_2PO_4 in water (B) as 1.0 mL/min. Gradient of eluent: 10% (A)/90% (B) for 3 min, from 10% (A)/90% (B) to 80% (A)/20% (B) for 17 min, 80% (A)/20% (B) for 5 min, from 80% (A)/20% (B) to 10% (A)/90% (B) for 1 min, and 10% (A)/90% (B) for 4 min. The high-resolution mass spectra (HRMS) and low-resolution mass spectra (LRMS) were recorded as fast atom bombardment (FAB). Flash column chromatography was performed on silica gel (Kieselgel 60, 230–400 mesh, Merck). Unless otherwise noted, materials were obtained from commercial suppliers and were used without purification. All solvents were purified and dried by standard techniques just before use.

Ligand Synthesis and Characterization. D-Erythrono-1,4-lactone was protected as the 2,3-acetonide under the standard conditions, which was reduced with diisobutylaluminum hydride (DIBAL-H) to afford lactol **3**.[28,29] Acetylation of lactol **3** afforded the glycosyl donor **4**.[29] Condensation of **4** with silylated 6-chloropurine under the Vorbrüggen[30] conditions using TMSOTf as a Lewis acid yielded the protected β-nucleoside **5** as a single stereoisomer.[15,29] Treatment of **5** with 1 N HCl followed by protection of resulting diol with a *t*-butyldimethylsilyl (TBS) group afforded the di-O-TBS ether, which was subjected to the iodination[31] at C2 and C8 positions using freshly prepared LiTMP to produce 2,8-diiodo-6-chloropurine derivative **6**. Sonogashira coupling[32,33] of **6** with 1-hexyne in the presence of tetrakis(triphenylphosphine) palladium and cesium carbonate yielded C2-hexynyl derivative **7** as the major regioisomer. Palladium-catalyzed Stille coupling[34] of **7** with 2-tributylstannylthiophene yielded the C8-thienyl derivative **8** after desilylation. Compound **8** was treated with ammonia to afford **2** (LJ-4517). Additional details of ligand synthesis and characterization are provided in the Supporting Information.

Protein Expression and Purification. The human A_{2A} adenosine receptor gene (UniProt ID: P29274) was optimized for insect cell expression and modified for crystallization to obtain the A_{2A}AR-STaR2-*b*RIL construct (C-terminal truncation: 317–412; ICL3-*b*RIL fusion replacing residues 208–218; mutations: A54L, T88A, R107A, K122A, N154A, L202A, L235A, V239A, and S277A). The residue S277 was restored in the A_{2A}AR-STaR2-S277-*b*RIL construct by site-directed mutagenesis using oligonucleotides (IDT) with internal mismatches and AccuPrime Pfx polymerase (Thermo Fisher Scientific) and verified by Sanger sequencing (Genewiz). Each of the constructs was inserted in a modified pFastBac1 vector (Invitrogen) containing an influenza hemagglutinin (HA) signaling peptide and a FLAG tag at the N-terminus and a 10× His tag at the C-terminus of the inserted gene. Chimeric receptors were expressed in *Spodoptera frugiperda* (Sf9) insect cells using the Bac-to-bac baculovirus expression system (Invitrogen). Cells with a density of (2–3) × 10^6 cells mL^{-1} were infected with baculovirus at 27 °C at a multiplicity of infection of 5, harvested by centrifugation 48 h post infection, and stored at −80 °C until use. The membrane fraction was isolated from 1 L of biomass using repeated Dounce homogenization and ultracentrifugation (25 min, 43,000*g*, 4 °C) in hypotonic (twice; 10 mM HEPES (pH 7.5), 10 mM $MgCl_2$, and 20 mM KCl) and

https://doi.org/10.1021/acs.jmedchem.2c00462
J. Med. Chem. 2022, 65, 11648−11657

hypertonic (three times; 10 mM HEPES (pH 7.5), 10 mM $MgCl_2$, 20 mM KCl, and 1 M NaCl) buffers.

Washed membranes were incubated in hypotonic buffer in the presence of 2 mg mL^{-1} iodoacetamide and 2 mM theophylline (Sigma-Aldrich) for 20 min at 4 °C, and the receptor was subsequently extracted from membranes in a volume of 50 mL by addition of 2× solubilization buffer (100 mM HEPES (pH 7.5), 250 mM NaCl, 0.5% (w/v) *n*-dodecyl-β-D-maltopyranoside (DDM, Anatrace), and 0.05% (w/v) cholesterol hemisuccinate (CHS, Sigma-Aldrich)) for 2.5 h. Unsolubilized membranes were separated by centrifugation (50 min, 60,000*g*, 4 °C). The supernatant was incubated overnight at 4 °C with 1 mL of Talon (immobilized metal affinity chromatography, IMAC) resin (Clontech) in the presence of 150 mM NaCl and 20 mM imidazole. After incubation, the sample was washed on a gravity column (Bio-Rad) with 10 column volumes (cv) of wash buffer 1 (50 mM HEPES (pH 7.5), 800 mM NaCl, 25 mM imidazole (pH 7.5), 10 mM $MgCl_2$, 0.05%/0.01% (w/v) DDM/CHS, and 100 μM **2**) followed by 5 cv of wash buffer 2 (50 mM HEPES (pH 7.5), 150 mM NaCl, 50 mM imidazole, 0.025%/0.005% (w/v) DDM/CHS, and 100 μM **2**). The sample was eluted in 3 cv of elution buffer (50 mM HEPES (pH 7.5), 150 mM NaCl, 250 mM imidazole (pH 7.5), 0.025%/0.005% (w/v) DDM/CHS, and 100 μM **2**) and concentrated to a volume of 20 μL using an Amicon centrifugal filter with 100 kDa molecular weight cutoff (Millipore).

Lipidic Cubic Phase Crystallization. The receptor was reconstituted into the lipidic cubic phase (LCP) by mixing two volumes of purified receptor (30 mg mL^{-1}) with three volumes of molten monoolein/cholesterol (9:1 w/w using coupled gas-tight 100 μL syringes (Hamilton)).[35] LCP boli (40 nL) were dispensed and overlaid with 800 nL of precipitant in 96-well LCP glass sandwich plates (Marienfeld) using the NT8-LCP system (Formulatrix). Crystallization hits were obtained in 0.1 M HEPES (pH 5.3), 0.05 M sodium thiocyanate, 30% PEG400, and 2% (v/v) 2,2,2-trifluoroethanol (Hampton Research). Crystals appeared within 6 days after setup and reached their maximum size of 50 × 10 × 3 μm in the case of the A_{2A}AR-STaR2-*b*RIL construct and within 2 days with the maximum size of 15 × 10 × 2 μm for A_{2A}AR-STaR2-S277-*b*RIL (Figure S1). Crystals were harvested directly from LCP using 50 μm micromounts (MiTeGen) and flash-frozen in liquid nitrogen.

Diffraction Data Collection and Structure Determination. X-ray diffraction data for A_{2A}AR-STaR2-*b*RIL/compound **2** and A_{2A}AR-STaR2-S277-*b*RIL/compound **2** were collected at the 23ID-B beamline of the Advanced Photon Source, Argonne, IL, equipped with a Dectris Eiger 16M detector using a 10 μm minibeam at a wavelength of 1.0330 Å, 0.1° oscillation, and 0.2 s exposure time. Crystals were located and centered using the beam rastering approach as previously described.[36] To limit radiation damage effects, the sample was shifted to a new position after collecting 100 images.

Diffraction images were indexed, integrated, scaled, and merged using HKL2000.[37] A total of six crystals were used for A_{2A}AR-STaR2-S277-*b*RIL/compound **2**, and 17 crystals were used for A_{2A}AR-STaR2-*b*RIL/compound **2** structure determination. Initial phases for A_{2A}AR-StaR2-*b*RIL/compound **2** were obtained by the molecular replacement (MR) method with Phaser[38] using the receptor and *b*RIL portions of the A_{2A}AR-*b*RIL/ZM-241385 structure (PDB ID: 4EIY) as independent search models. Refinement was carried out using iterative cycles with Buster[39] and Phenix[40] followed by manual examination and adjustments of the refined structures in the program COOT[41] with both 2mFo-DFc and mFo-DFc maps. For structure determination of A_{2A}AR-STaR2-S277-*b*RIL/compound **2**, the final structure of A_{2A}AR-STaR2-*b*RIL/compound **2** was used as a search model for molecular replacement. Final data collection and refinement statistics are shown in Table S1.

Radioligand Binding Assay. Radioligand binding assays were performed using cell membranes prepared from CHO cells stably expressing WT or mutant human A_{2A}ARs. For saturation binding experiments, increasing concentrations (0.2 to 20 nM) of [3*H*]4-[2-[7-amino-2-(2-furyl)-1,2,4-triazolo[1,5-*a*][1,3,5]triazin-5-yl-amino]-ethylphenol ([^{3}H]ZM-241385) were incubated with membranes (15 μg of protein) at 25 °C for 60 min in a total of 200 μL of Tris−HCl buffer (50 mM, pH 7.5) containing 10 mM $MgCl_2$. A saturated concentration (30 μM) of the antagonist 8-[4-[[[[(2-aminoethyl)-amino]carbonyl]methyl]oxy]phenyl]-1,3-dipropylxanthine (XAC) was used to determine the nonspecific binding. For displacement binding experiments, increasing concentrations of ligands were incubated with [^{3}H]ZM-241385 (1.2 nM) and membrane preparations at 25 °C for 60 min. Binding reactions were terminated by filtration through Whatman GF/B filters under reduced pressure using an MT-24 cell harvester (Brandell, Gaithersburg, MD, USA) and followed by washing twice with 5 mL of cold Tris−HCl buffer. Radioactivity was measured using a scintillation counter (Tri-Carb 2810TR). Radioligand binding assays for A_1AR and A_3AR were performed by the procedure described in our previous work.[12] Competitive binding assay for A_{2B}AR was performed in accordance with the published procedure.[42] Data were analyzed using GraphPad Prism 8.1.0. IC_{50} values were converted to K_i values using the Cheng−Prusoff equation.[43]

cAMP Accumulation Assay. For the cAMP production assay, CHO cells were plated in 96-well plates in 100 μL of medium. Cells were cultured in a mixture of DMEM (50%) and F12 medium (50%) supplied with 10% fetal bovine serum, 100 units mL^{-1} penicillin, 100 μg mL^{-1} streptomycin, and 2 μmol mL^{-1} glutamine. After overnight culture, cells were treated with adenosine deaminase (3 units mL^{-1}) and the phosphodiesterase inhibitor rolipram (10 μM) for 30 min before the addition of agonists and incubated at 37 °C for another 20 min. The standard full agonist used was CGS21680 (2-[*p*-(2-carboxyethyl)phenyl-ethylamino]-5′-*N*-ethylcarboxamidoadenosine). For the test of an antagonist activity, 300 nM LJ-4517 was preincubated for 20 min before the addition of agonists. The reaction was terminated by removal of the supernatant, and cells were lysed upon the addition of 50 μL of lysis buffer (0.3% Tween-20). An AlphaScreen cAMP Kit (PerkinElmer, Waltham, MA) was used for determining the amount of cAMP following manufacturer's instructions.

Molecular Dynamics (MD) Simulation. Using the crystal structure of A_{2A}AR-STaR2-S277-*b*RIL/compound **2** (PDB ID: 8CU6), the input receptor structure was generated with the WT full sequence of human A_{2A}AR. The Membrane Builder module[44] in CHARMM-GUI (www.charmm-gui.org, accessed Jul 01, 2022)[45] was used to insert the receptor structure into the lipid bilayer system, consisting of 136 POPC (1-palmitoyl-2-oleoyl-*sn*-glycero-3-phosphocholine) molecules. The prepared system was solvated with a water box (13,225 TIP3 water molecules) and neutralized with ions to make 150 mM salt concentration (34 Na^+ molecules and 43 Cl^- molecules). The MD simulations were performed using Gromacs v.2018.4[46] with the CHARMM36 force field.[47] The force field for the ligand molecule was generated by the CHARMM general force field (CGenFF) program.[48] The pre-equilibration process was conducted under an NVT (constant particle number, volume, and temperature) ensemble for the 10 ns simulation time, followed by 40 ns simulation under an NPT (constant particle number, pressure, and temperature) ensemble for system equilibration. Then, the production run was performed under NPT for 1000 ns. A time step of 2 fs was used in all simulations, and the data were sampled every 1 ns for the analysis and movie making.

■ ASSOCIATED CONTENT

Supporting Information

The Supporting Information is available free of charge at https://pubs.acs.org/doi/10.1021/acs.jmedchem.2c00462.

Ligand synthesis and characterization details and additional tables/figures (PDF)

Movie file of molecular dynamics simulation (MPG)

Molecular formula strings (CSV)

Crystallographic data of A_{2A}AR-STaR2-*b*RIL/LJ-4517 (**2**) (PDB)

Crystallographic data of A_{2A}AR-STaR2-S277-*b*RIL/LJ-4517 (**2**) (PDB)

https://doi.org/10.1021/acs.jmedchem.2c00462
J. Med. Chem. 2022, 65, 11648−11657

Accession Codes

Coordinates and structure factors have been deposited in the Protein Data Bank (PDB) under the accession codes 8CU6 (A_{2A}AR-STaR2-S277-*b*RIL/LJ-4517 (**2**)) and 8CU7 (A_{2A}AR-STaR2-*b*RIL/LJ-4517 (**2**)). Authors will release the atomic coordinates and experimental data upon article publication.

AUTHOR INFORMATION

Corresponding Authors

Lak Shin Jeong − *Research Institute of Pharmaceutical Sciences, College of Pharmacy, Seoul National University, Seoul 08826, Republic of Korea;* orcid.org/0000-0002-3441-707X; Email: lakjeong@snu.ac.kr

Sun Choi − *Global AI Drug Discovery Center, College of Pharmacy and Graduate School of Pharmaceutical Sciences, Ewha Womans University, Seoul 03760, Republic of Korea;* orcid.org/0000-0002-7669-7954; Email: sunchoi@ewha.ac.kr

Vadim Cherezov − *Department of Chemistry, University of Southern California, Los Angeles, California 90089, United States; Bridge Institute, University of Southern California, Los Angeles, California 90089, United States;* orcid.org/0000-0002-5265-3914; Email: cherezov@usc.edu

Authors

Anna Shiriaeva − *Department of Chemistry, University of Southern California, Los Angeles, California 90089, United States; Bridge Institute, University of Southern California, Los Angeles, California 90089, United States*

Daejin Park − *Department of Pharmacology, Kosin University College of Medicine, Busan 49267, Republic of Korea*

Gyudong Kim − *Research Institute of Pharmaceutical Sciences, College of Pharmacy, Seoul National University, Seoul 08826, Republic of Korea; College of Pharmacy & Research Institute of Drug Development, Chonnam National University, Gwangju 61186, Republic of Korea;* orcid.org/0000-0002-4894-951X

Yoonji Lee − *College of Pharmacy, Chung-Ang University, Seoul 06974, Republic of Korea;* orcid.org/0000-0002-2494-5792

Xiyan Hou − *Research Institute of Pharmaceutical Sciences, College of Pharmacy, Seoul National University, Seoul 08826, Republic of Korea*

Dnyandev B. Jarhad − *Research Institute of Pharmaceutical Sciences, College of Pharmacy, Seoul National University, Seoul 08826, Republic of Korea*

Gibae Kim − *Research Institute of Pharmaceutical Sciences, College of Pharmacy, Seoul National University, Seoul 08826, Republic of Korea*

Jinha Yu − *Research Institute of Pharmaceutical Sciences, College of Pharmacy, Seoul National University, Seoul 08826, Republic of Korea*

Young Eum Hyun − *Research Institute of Pharmaceutical Sciences, College of Pharmacy, Seoul National University, Seoul 08826, Republic of Korea*

Woomi Kim − *Department of Pharmacology, Kosin University College of Medicine, Busan 49267, Republic of Korea*

Zhan-Guo Gao − *Laboratory of Bioorganic Chemistry, National Institute of Diabetes and Digestive and Kidney Disease, National Institutes of Health, Bethesda, Maryland 20892, United States*

Kenneth A. Jacobson − *Laboratory of Bioorganic Chemistry, National Institute of Diabetes and Digestive and Kidney Disease, National Institutes of Health, Bethesda, Maryland 20892, United States;* orcid.org/0000-0001-8104-1493

Gye Won Han − *Department of Chemistry, University of Southern California, Los Angeles, California 90089, United States; Bridge Institute, University of Southern California, Los Angeles, California 90089, United States*

Raymond C. Stevens − *Department of Chemistry, University of Southern California, Los Angeles, California 90089, United States; Bridge Institute, University of Southern California, Los Angeles, California 90089, United States; Structure Therapeutics, South San Francisco, California 94080, United States*

Complete contact information is available at: https://pubs.acs.org/10.1021/acs.jmedchem.2c00462

Author Contributions

○A.S., D.P., G.K., and Y.L. contributed equally to this work.

Author Contributions

A.S. and D.P. designed the expression constructs and performed purification, crystallization, data collection, and structure determination and analysis. G.K., X.H., D.B.J., G.K., J.Y., Y.E.H., and L.S.J. designed and synthesized compound **2** (LJ-4517). G.W.H. performed structure refinement. G.W.H. and W.K. conducted the structural analysis. K.A.J. and Z.-G.G. performed functional studies. Y.L. and S.C. performed the structural analysis and MD simulations. R.C.S. helped shape the research and provided facilities for protein expression. G.W.H. and S.C. initiated the project. V.C., S.C., and L.S.J. supervised the studies. A.S., D.P., K.A.J., Y.L., S.C., V.C., G.K., and L.S.J. wrote the article with inputs from all co-authors. All authors have given approval to the final version of the manuscript.

Funding

This work was supported by the National Science Foundation (NSF) BioXFEL Science and Technology Center award 1231306 and National Institutes of Health (NIH) grant R35 GM127086 to V.C., the Mid-career Researcher Program NRF-2021R1A2B020015441 to L.S.J., NRF-2020R1A2C2101636 and Bio & Medical Technology Development Program NRF-2022M3E5F3080873 funded by the Ministry of Science and ICT (MSIT) through the National Research Foundation of Korea (NRF) to S.C., the Young Researcher Program NRF-2022R1C1C1007409 to Y.L., and the NIDDK Intramural Research Program (ZIADK31117).

Notes

The authors declare no competing financial interest.

ACKNOWLEDGMENTS

GM/CA@APS was funded by the National Cancer Institute (ACB-12002) and the National Institute of General Medical Sciences (AGM-12006, P30GM138396). This research used resources of the Advanced Photon Source, a U.S. Department of Energy (DOE) Office of Science User Facility operated for the DOE Office of Science by Argonne National Laboratory under contract no. DE-AC02-06CH11357. The Eiger 16M detector at GM/CA-XSD was funded by NIH grant S10 OD012289. We thank the Korea Institute of Science and Technology Information (KISTI) National Supercomputing Center for providing the computing resources (KSC-2020-CRE-0359).

ABBREVIATIONS

AR, adenosine receptor; GPCR, G protein-coupled receptor; MD, molecular dynamics

REFERENCES

(1) Fredholm, B. B.; AP, I. J.; Jacobson, K. A.; Klotz, K. N.; Linden, J. International Union of Pharmacology. XXV. Nomenclature and classification of adenosine receptors. *Pharmacol. Rev.* **2001**, *53*, 527−552.

(2) Borea, P. A.; Gessi, S.; Merighi, S.; Vincenzi, F.; Varani, K. Pharmacology of adenosine receptors: The state of the art. *Physiol. Rev.* **2018**, *98*, 1591−1625.

(3) Baroud, M.; Lepeltier, E.; Thepot, S.; El-Makhour, Y.; Duval, O. The evolution of nucleosidic analogues: self-assembly of prodrugs into nanoparticles for cancer drug delivery. *Nanoscale Adv* **2021**, *3*, 2157−2179.

(4) Lin, X.; Liang, C.; Zou, L.; Yin, Y.; Wang, J.; Chen, D.; Lan, W. Advance of structural modification of nucleosides scaffold. *Eur. J. Med. Chem.* **2021**, *214*, No. 113233.

(5) Blum, D.; Hourez, R.; Galas, M. C.; Popoli, P.; Schiffmann, S. N. Adenosine receptors and Huntington's disease: implications for pathogenesis and therapeutics. *Lancet Neurol.* **2003**, *2*, 366−374.

(6) Schwarzschild, M. A.; Agnati, L.; Fuxe, K.; Chen, J. F.; Morelli, M. Targeting adenosine A2A receptors in Parkinson's disease. *Trends Neurosci.* **2006**, *29*, 647−654.

(7) Benarroch, E. E. Adenosine and its receptors: multiple modulatory functions and potential therapeutic targets for neurologic disease. *Neurology* **2008**, *70*, 231−236.

(8) Leone, R. D.; Lo, Y. C.; Powell, J. D. A2aR antagonists: Next generation checkpoint blockade for cancer immunotherapy. *Comput. Struct. Biotechnol. J.* **2015**, *13*, 265−272.

(9) Gessi, S.; Bencivenni, S.; Battistello, E.; Vincenzi, F.; Colotta, V.; Catarzi, D.; Varano, F.; Merighi, S.; Borea, P. A.; Varani, K. Inhibition of A2A adenosine receptor signaling in cancer cells proliferation by the novel antagonist TP455. *Front. Pharmacol.* **2017**, *8*, 888.

(10) de Lera Ruiz, M.; Lim, Y. H.; Zheng, J. Adenosine A2A receptor as a drug discovery target. *J. Med. Chem.* **2014**, *57*, 3623−3650.

(11) Jacobson, K. A.; Merighi, S.; Varani, K.; Borea, P. A.; Baraldi, S.; Tabrizi, M. A.; Romagnoli, R.; Baraldi, P. G.; Ciancetta, A.; Tosh, D. K.; Gao, Z. G.; Gessi, S. A3 adenosine receptors as modulators of inflammation: From medicinal chemistry to therapy. *Med. Res. Rev.* **2018**, *38*, 1031−1072.

(12) Lee, Y.; Hou, X. Y.; Lee, J. H.; Nayak, A.; Alexander, V.; Sharma, P. K.; Chang, H.; Phan, K.; Gao, Z. G.; Jacobson, K. A.; Choi, S.; Jeong, L. S. Subtle chemical changes cross the boundary between agonist and antagonist: New A3 adenosine receptor homology models and structural network analysis can predict this boundary. *J. Med. Chem.* **2021**, *64*, 12525−12536.

(13) Jaakola, V. P.; Griffith, M. T.; Hanson, M. A.; Cherezov, V.; Chien, E. Y.; Lane, J. R.; Ijzerman, A. P.; Stevens, R. C. The 2.6 angstrom crystal structure of a human A2A adenosine receptor bound to an antagonist. *Science* **2008**, *322*, 1211−1217.

(14) Xu, F.; Wu, H.; Katritch, V.; Han, G. W.; Jacobson, K. A.; Gao, Z. G.; Cherezov, V.; Stevens, R. C. Structure of an agonist-bound human A2A adenosine receptor. *Science* **2011**, *332*, 322−327.

(15) Hou, X.; Majik, M. S.; Kim, K.; Pyee, Y.; Lee, Y.; Alexander, V.; Chung, H. J.; Lee, H. W.; Chandra, G.; Lee, J. H.; Park, S. G.; Choi, W. J.; Kim, H. O.; Phan, K.; Gao, Z. G.; Jacobson, K. A.; Choi, S.; Lee, S. K.; Jeong, L. S. Structure-activity relationships of truncated C2- or C8-substituted adenosine derivatives as dual acting A2A and A3 adenosine receptor ligands. *J. Med. Chem.* **2012**, *55*, 342−356.

(16) Ballesteros, J. A.; Weinstein, H. [19] Integrated methods for the construction of three-dimensional models and computational probing of structure-function relations in G protein-coupled receptors. *Methods Neurosci.* **1995**, *25*, 366−428.

(17) Liu, W.; Chun, E.; Thompson, A. A.; Chubukov, P.; Xu, F.; Katritch, V.; Han, G. W.; Roth, C. B.; Heitman, L. H.; AP, I. J.; Cherezov, V.; Stevens, R. C. Structural basis for allosteric regulation of GPCRs by sodium ions. *Science* **2012**, *337*, 232−236.

(18) Cheng, R. K. Y.; Segala, E.; Robertson, N.; Deflorian, F.; Dore, A. S.; Errey, J. C.; Fiez-Vandal, C.; Marshall, F. H.; Cooke, R. M. Structures of human A1 and A2A adenosine receptors with xanthines reveal determinants of selectivity. *Structure* **2017**, *25*, 1275−1285.e4.

(19) Lebon, G.; Warne, T.; Edwards, P. C.; Bennett, K.; Langmead, C. J.; Leslie, A. G.; Tate, C. G. Agonist-bound adenosine A2A receptor structures reveal common features of GPCR activation. *Nature* **2011**, *474*, 521−525.

(20) Zhukov, A.; Andrews, S. P.; Errey, J. C.; Robertson, N.; Tehan, B.; Mason, J. S.; Marshall, F. H.; Weir, M.; Congreve, M. Biophysical mapping of the adenosine A2A receptor. *J. Med. Chem.* **2011**, *54*, 4312−4323.

(21) Jespers, W.; Schiedel, A. C.; Heitman, L. H.; Cooke, R. M.; Kleene, L.; van Westen, G. J. P.; Gloriam, D. E.; Muller, C. E.; Sotelo, E.; Gutierrez-de-Teran, H. Structural mapping of adenosine receptor mutations: Ligand binding and signaling mechanisms. *Trends Pharmacol. Sci.* **2018**, *39*, 75−89.

(22) Borodovsky, A.; Barbon, C. M.; Wang, Y.; Ye, M.; Prickett, L.; Chandra, D.; Shaw, J.; Deng, N.; Sachsenmeier, K.; Clarke, J. D.; Linghu, B.; Brown, G. A.; Brown, J.; Congreve, M.; Cheng, R. K.; Dore, A. S.; Hurrell, E.; Shao, W.; Woessner, R.; Reimer, C.; Drew, L.; Fawell, S.; Schuller, A. G.; Mele, D. A. Small molecule AZD4635 inhibitor of A2AR signaling rescues immune cell function including CD103(+) dendritic cells enhancing anti-tumor immunity. *J. Immunother. Cancer* **2020**, *8*, No. e000417.

(23) Rucktooa, P.; Cheng, R. K. Y.; Segala, E.; Geng, T.; Errey, J. C.; Brown, G. A.; Cooke, R. M.; Marshall, F. H.; Dore, A. S. Towards high throughput GPCR crystallography: In meso soaking of adenosine A2A receptor crystals. *Sci. Rep.* **2018**, *8*, 41.

(24) Lee, M. Y.; Geiger, J.; Ishchenko, A.; Han, G. W.; Barty, A.; White, T. A.; Gati, C.; Batyuk, A.; Hunter, M. S.; Aquila, A.; Boutet, S.; Weierstall, U.; Cherezov, V.; Liu, W. Harnessing the power of an X-ray laser for serial crystallography of membrane proteins crystallized in lipidic cubic phase. *IUCrJ* **2020**, *7*, 976−984.

(25) Sun, B.; Bachhawat, P.; Chu, M. L.; Wood, M.; Ceska, T.; Sands, Z. A.; Mercier, J.; Lebon, F.; Kobilka, T. S.; Kobilka, B. K. Crystal structure of the adenosine A2A receptor bound to an antagonist reveals a potential allosteric pocket. *Proc. Natl. Acad. Sci. U. S. A.* **2017**, *114*, 2066−2071.

(26) Lee, Y.; Basith, S.; Choi, S. Recent Advances in Structure-Based Drug Design Targeting Class A G Protein-Coupled Receptors Utilizing Crystal Structures and Computational Simulations. *J. Med. Chem.* **2018**, *61*, 1−46.

(27) Lee, Y.; Lazim, R.; Macalino, S. J. Y.; Choi, S. Importance of protein dynamics in the structure-based drug discovery of class A G protein-coupled receptors (GPCRs). *Curr Opin Struc Biol* **2019**, *55*, 147−153.

(28) de Napoli, L.; Messere, A.; Palomba, D.; Piccialli, G.; Piccialli, V.; Evidente, A. Studies toward the synthesis of pinolidoxin, a phytotoxic nonenolide from the fungus Ascochyta pinodes. Determination of the configuration at the C-7, C-8, and C-9 chiral centers and stereoselective synthesis of the C(6)-C(18) fragment. *J. Org. Chem.* **2000**, *65*, 3432−3442.

(29) Pal, S.; Choi, W. J.; Choe, S. A.; Heller, C. L.; Gao, Z. G.; Chinn, M.; Jacobson, K. A.; Hou, X.; Lee, S. K.; Kim, H. O.; Jeong, L. S. Structure-activity relationships of truncated adenosine derivatives as highly potent and selective human A3 adenosine receptor antagonists. *Bioorg. Med. Chem.* **2009**, *17*, 3733−3738.

(30) Vorbrüggen, H.; Ruh-Pohlenz, C. Synthesis of nucleosides. *Org. React.* **2004**, *55*, 1−630.

(31) Ibrahim, N.; Chevot, F.; Legraverend, M. Regioselective Sonogashira cross-coupling reactions of 6-chloro-2,8-diiodo-9-THP-9H-purine with alkyne derivatives. *Tetrahedron Lett.* **2011**, *52*, 305−307.

(32) Sonogashira, K. Development of Pd-Cu catalyzed cross-coupling of terminal acetylenes with sp2-carbon halides. *J. Organomet. Chem.* **2002**, *653*, 46−49.

https://doi.org/10.1021/acs.jmedchem.2c00462
J. Med. Chem. 2022, 65, 11648−11657

(33) Chinchilla, R.; Najera, C. The Sonogashira reaction: a booming methodology in synthetic organic chemistry. *Chem. Rev.* **2007**, *107*, 874−922.
(34) Stille, J. K. The palladium-catalyzed cross-coupling reactions of organotin reagents with organic electrophiles. *Angew. Chem., Int. Ed. Engl.* **1986**, *25*, 508−524.
(35) Caffrey, M.; Cherezov, V. Crystallizing membrane proteins using lipidic mesophases. *Nat. Protoc.* **2009**, *4*, 706−731.
(36) Cherezov, V.; Hanson, M. A.; Griffith, M. T.; Hilgart, M. C.; Sanishvili, R.; Nagarajan, V.; Stepanov, S.; Fischetti, R. F.; Kuhn, P.; Stevens, R. C. Rastering strategy for screening and centring of microcrystal samples of human membrane proteins with a sub-10 microm size X-ray synchrotron beam. *J. R. Soc., Interface* **2009**, *6*, S587−S597.
(37) Otwinowski, Z.; Minor, W. Processing of X-ray diffraction data collected in oscillation mode. *Methods Enzymol.* **1997**, *276*, 307−326.
(38) McCoy, A. J.; Grosse-Kunstleve, R. W.; Adams, P. D.; Winn, M. D.; Storoni, L. C.; Read, R. J. Phaser crystallographic software. *J. Appl. Crystallogr.* **2007**, *40*, 658−674.
(39) Smart, O. S.; Womack, T. O.; Flensburg, C.; Keller, P.; Paciorek, W.; Sharff, A.; Vonrhein, C.; Bricogne, G. Exploiting structure similarity in refinement: automated NCS and target-structure restraints in BUSTER. *Acta Crystallogr., Sect. D: Biol. Crystallogr.* **2012**, *68*, 368−380.
(40) Liebschner, D.; Afonine, P. V.; Baker, M. L.; Bunkoczi, G.; Chen, V. B.; Croll, T. I.; Hintze, B.; Hung, L. W.; Jain, S.; McCoy, A. J.; Moriarty, N. W.; Oeffner, R. D.; Poon, B. K.; Prisant, M. G.; Read, R. J.; Richardson, J. S.; Richardson, D. C.; Sammito, M. D.; Sobolev, O. V.; Stockwell, D. H.; Terwilliger, T. C.; Urzhumtsev, A. G.; Videau, L. L.; Williams, C. J.; Adams, P. D. Macromolecular structure determination using X-rays, neutrons and electrons: recent developments in Phenix. *Acta Crystallogr., Sect. D: Struct. Biol.* **2019**, *75*, 861−877.
(41) Emsley, P.; Lohkamp, B.; Scott, W. G.; Cowtan, K. Features and development of Coot. *Acta Crystallogr., Sect. D: Biol. Crystallogr.* **2010**, *66*, 486−501.
(42) Auchampach, J. A.; Kreckler, L. M.; Wan, T. C.; Maas, J. E.; van der Hoeven, D.; Gizewski, E.; Narayanan, J.; Maas, G. E. Characterization of the A2B adenosine receptor from mouse, rabbit, and dog. *J. Pharmacol. Exp. Ther.* **2009**, *329*, 2−13.
(43) Cheng, Y.; Prusoff, W. H. Relationship between the inhibition constant (K1) and the concentration of inhibitor which causes 50 per cent inhibition (I50) of an enzymatic reaction. *Biochem. Pharmacol.* **1973**, *22*, 3099−3108.
(44) Wu, E. L.; Cheng, X.; Jo, S.; Rui, H.; Song, K. C.; Davila-Contreras, E. M.; Qi, Y.; Lee, J.; Monje-Galvan, V.; Venable, R. M.; Klauda, J. B.; Im, W. CHARMM-GUI Membrane Builder toward realistic biological membrane simulations. *J. Comput. Chem.* **2014**, *35*, 1997−2004.
(45) Jo, S.; Kim, T.; Iyer, V. G.; Im, W. CHARMM-GUI: a web-based graphical user interface for CHARMM. *J. Comput. Chem.* **2008**, *29*, 1859−1865.
(46) Abraham, M. J.; Murtola, T.; Schulz, R.; Páll, S.; Smith, J. C.; Hess, B.; Lindahl, E. GROMACS: High performance molecular simulations through multi-level parallelism from laptops to supercomputers. *SoftwareX* **2015**, *1-2*, 19−25.
(47) Huang, J.; MacKerell, A. D., Jr. CHARMM36 all-atom additive protein force field: validation based on comparison to NMR data. *J. Comput. Chem.* **2013**, *34*, 2135−2145.
(48) Vanommeslaeghe, K.; MacKerell, A. D., Jr. Automation of the CHARMM General Force Field (CGenFF) I: bond perception and atom typing. *J. Chem. Inf. Model.* **2012**, *52*, 3144−3154.

https://doi.org/10.1021/acs.jmedchem.2c00462
J. Med. Chem. 2022, 65, 11648−11657